University of Bristol - Explore Bristol Research
General rights

Post-buckling analysis of variable-angle tow composite plates using Koiter's approach and the finite element method

A Madeo[a,*], RMJ Groh[b], G Zucco[a], PM Weaver[b], G Zagari[a], R Zinno[a]

[a]*DIMES, University of Calabria, Ponte P. Bucci Cubo, 87036 Rende (Cosenza), Italy*
[b]*ACCIS, University of Bristol, Queen's Building, University Walk, Bristol, BS8 1 TR, UK*

Abstract

The design of lightweight structures is often driven by buckling phenomena. Increasing demands for fuel-efficient aircraft structures makes post-buckled designs attractive from a structural weight perspective. However, the need for reliable and efficient design tools that accurately model the emerging nonlinear post-buckled landscape, potentially one containing multiple branches, remains. With this aim, a previously derived flat shell element, MISS-4, is extended to the geometrically nonlinear analysis of variable-angle tow (VAT) composite plates using Koiter's asymptotic approach. The curvilinear fiber paths in VAT lamina open the design space for tailoring the buckling and post-buckling capability of plates and shells. A finite element implementation of Koiter's asymptotic approach allows the pre-critical and post-critical behavior of slender elastic structures to be evaluated in a computationally efficient manner. Its implementation uses a fourth-order expansion of the strain energy, and requires both the structural modeling and finite element discretization procedures to be, at least, of fourth order. The corotational approach adopted in the MISS-4 element readily fulfills this requirement by starting from a linear finite element discretization. VAT plates with prismatic fiber variations and different loading conditions are analyzed using the MISS-4 element and numerical results of the post-buckling paths are presented. The computed equilibrium paths are compared to benchmark results using the commercial finite element package ABAQUS, and strong asymptotic solutions of the differential equations. The results document the good accuracy and reliability of the proposed modeling approach, and also highlight the importance of multi-modal analysis when multiple buckling modes coincide as is the case in long plates, shells and other optimized thin-walled structures.

Keywords: Variable angle tow, mixed finite element, buckling, post-buckling, Koiter's method.

1. INTRODUCTION

In the analysis of slender elastic structures, the numerical implementation of Koiter's asymptotic method [1] allows a reliable evaluation of the post-buckling behavior. The method, its implementation and application are under investigation to this day [2–7]. The advantages of Koiter's asymptotic approach are apparent when multi-modal buckling interactions are to be accounted for. Furthermore, the sensitivity to imperfections, and therefore a realistic evaluation of the load carrying capacity of the structure, can be studied in a computationally efficient manner by combining Koiter's asymptotic approach with stochastic Monte Carlo simulations [8–12].

A finite element implementation of Koiter's asymptotic method was developed by Casciaro et al. [13, 14]. Initially, this method was applied to planar beam frames [15, 16] and simple plate assemblies [17]. The use of a corotational formulation [18, 19] allowed the simple extension of the underlying linear model to the geometrically nonlinear regime and permitted the straightforward computation of high-order strain

---

energy derivatives. As a result, the analysis could be extended to spatial beam frames [20] and general shell structures [21]. Recently, the formulation has been extended to laminate composite shell structures [9], particularly to cylindrical shells [22] and folded plate structures [10], and to cold formed steel structures [23]. By coupling the asymptotic method with a Monte Carlo engine, the effect of random imperfections on the first critical load of cylindrical shells in compression [22], and the erosion [24–26] of critical loads of cold formed sections have been investigated [23]. Recently, the method has been validated experimentally for composite beams [27] confirming the good accuracy and reliability of the approach.

Here, a general finite element for the pre-buckling, buckling and post-buckling analysis of variable-angle tow (VAT) plates using Koiter's asymptotic approach is proposed. Due to the increased design space for locally tailoring laminate stiffness, VAT composites are a promising technology for further improving the structural efficiency of engineering structures. In these variable stiffness structures, the fiber tows within a layer are not restricted to straight trajectories but can describe curvilinear paths. Numerous works have shown that tailoring the in-plane stiffness over the plate planform allows pre-buckling stresses to be redistributed to supported regions, thereby increasing the first critical buckling load [28–35].

Wu et al. [36] showed that the fiber orientations of flat VAT laminates can be tailored to reduce the stiffness knock-down in the post-critical regime compared to straight-fiber laminates. Furthermore, the optimal fiber paths for increasing buckling load also reduce the out-of-plane post-buckling displacements [37]. An interesting application of variable-stiffness composites is the reduction of the imperfection sensitivity of shell structures. It is well known in the engineering community that cylindrical shells are prone to collapse beyond the first critical load, and as a result of this instability, shell structures are extremely sensitive to geometric and loading imperfections. White and Weaver [38] showed that this imperfection sensitivity can be effectively eliminated by tailoring the fiber paths across the surface of cylindrical shells. Hence, stable plate-like post-buckling responses in cylindrical shells were documented for the first time.

Due to its modeling versatility and numerical robustness, most modeling work on the buckling of VAT structures has focused on using the finite element method (FEM) [30, 39–42]. At the same time, the pseudo-spectral differential quadrature method (DQM) has been shown to be a fast, accurate and computationally efficient technique for solving the variable-coefficient higher-order differential equations for buckling [33, 43] and post-buckling [35, 44] of VAT plates and cylindrical shells [45, 46].

White et al. [45] were the first to implement Koiter's asymptotic approach within a DQM framework. The asymptotic differential equations for the pre-buckling, buckling and initial post-buckling problem of constant stiffness curved panels were solved using the generalized DQM, while the orthogonality condition of the buckling and initial post-buckling mode shapes was enforced as an additional constraint equation using an integral quadrature approach. The overdetermined system was then solved using the Moore-Penrose generalized matrix inverse operation. This general approach was used in the optimization study of imperfection-insensitive cylindrical shells mentioned above, and by Groh and Weaver [46] in a minimum-mass optimization study of VAT wing panels with static failure constraints. Finally, Raju et al. [47] extended the numerical scheme beyond the initial post-buckling regime, and used the approach as the basis for an optimization scheme to minimize the end-shortening strain in the post-buckling regime.

The starting point of the present implementation of Koiter's asymptotic approach in the finite element method is the 3D shell element MISS-4 [48–50]. The use of a corotational reference frame allows the extension of the geometrically linear finite element into a nonlinear context. The fundamental equations of Koiter's asymptotic method are presented in Section 2. Derivations of the linear shell element MISS-4 are discussed in Section 3, and its extension to the geometrically nonlinear regime presented in Section 4. In Section 5, a number of different test cases with different VAT stacking sequences and loading conditions are presented and comparisons are made with benchmark models. In particular, the results have been compared with the Riks path-following algorithm [51] in the commercial code ABAQUS [52] and with the implementation of Koiter's approach in DQM [45]. Furthermore, this section highlights the importance of multi-modal expansions in Koiter's approach. Finally, conclusions are drawn in Section 6.

2. NONLINEAR ANALYSIS OF SLENDER ELASTIC STRUCTURES

The starting point of Koiter's asymptotic approach is the total potential energy functional $\Pi[u]$, where u are the configuration variables (i.e. displacements/stresses). In particular, we have

$$\Pi[u] = \Phi[u] - \lambda p u \tag{1}$$

where $\Phi[u]$ is the strain energy, λ the load control parameter and p the applied load. The solution to the problem is given by the stationarity condition of the total potential energy

$$\Pi[u] = \text{stat.} \tag{2}$$

which means that the first variation of the total potential energy must vanish. Hence,

$$\Pi'[u]\delta u = \Phi'[u]\delta u - \lambda p \delta u = 0 \quad \forall \delta u \tag{3}$$

where the prime denotes the Frèchet derivative with respect to configuration variable u, and the equilibrium Eq. (3) is generally nonlinear. Using the finite element method, Eq. (3) can be rewritten as

$$\delta u^T r[u, \lambda] = 0 \quad \forall \delta u \qquad r[u, \lambda] = (s[u] - \lambda p) \tag{4}$$

with $u = \mathcal{L}u$ and $p = \mathcal{L}p$, where $\mathcal{L}$ is a suitable interpolation operator, and $s[u]$ and p represent the internal and external load vectors, respectively. The solution of Eq. (4), and therefore the equilibrium path, can be obtained either by means of a path-following approach or an asymptotic approach.

The path-following [51] approach is widely used as a solution scheme because of its general applicability to a wide array of nonlinear systems. Disadvantages include the computational cost, which is directly related to the number of variables in the FEM discretization (i.e. the dimension u); the need to perform separate analyses in the case of small modifications (i.e. imperfections) of the load and/or geometry; and difficulties associated with following post-critical branches at coincident, or near-coincident, critical loads.

On the other hand, in the asymptotic analysis [1], the equilibrium path is obtained in an approximate fashion through an asymptotic expansion of parameters ξ_i for $i = 0 \ldots m$. Starting from a known expansion point $\{u_0, \lambda_0\}$, we have:

$$u = u_0 + \sum_{i=0}^{n} \xi_i \dot{u}_i + \frac{1}{2} \sum_{i,j=0}^{m} \xi_i \xi_j \ddot{u}_{ij} + \cdots + O(\xi_i^k) \quad , \quad \lambda = \lambda_0 + \sum_{i=0}^{n} \xi_i \dot{\lambda}_i + \frac{1}{2} \sum_{i,j=0}^{m} \xi_i \xi_j \ddot{\lambda}_{ij} + \cdots + O(\xi_i^k) \tag{5}$$

where the superimposed $(\cdot)$ denotes differentiation with respect to ξ. By invoking the fundamental lemma of the calculus of variations, the nonlinear system of Eqs. (4) can be rewritten as

$$r[\xi, \lambda] = 0 \tag{6}$$

with vector ξ collecting the ξ_i expansion parameters. The nonlinear system Eq. (6) is generally defined by a reduced number of variables. In practical contexts the expansion order m is of order 10^1. Once all unknowns in Eq. (5) are determined for the so-called 'perfect structure', the solution for deviations in the assumed load and geometrical imperfections only require the solution of Eq. (6). Thus, the reduced order of the asymptotic method allows the straightforward computation of thousands of imperfections at low computational cost.

2.1. Koiter's approach fundamental equations: Casciaro's quadratic algorithm

In the following, Koiter's asymptotic approach as proposed by Casciaro [13, 14] in the context of the FEM is employed. This implementation is also know as the *quadratic algorithm* [13] and has been developed

over the last thirty years.

The analysis procedure can be summarized as follows:

- First, the *fundamental path* (pre-critical path) is assumed to be a linear combination

$$u^f[\lambda] = u_0 + \lambda \hat{u} \tag{7}$$

where u_0 is an initial known configuration, and $\hat{u} = du/d\lambda$ is computed from the linear algebraic equation

$$K_0 \hat{u} = \hat{p} \tag{8}$$

where $\hat{p}$ is a reference load vector, and K_0 is the the stiffness matrix evaluated at u_0, that is $K_0 = K[u_0]$.

- Second, a multi-modal buckling problem is solved to obtain a cluster of buckling loads λ_i, $i = 1 \ldots m$, and associated buckling modes $\dot{v}_i$ along $u^f[\lambda]$. Hence, the stability criterion

$$K[\lambda_i]\dot{v}_i = 0 \quad , \quad K[\lambda_i] = K[u_0 + \lambda_i \hat{u}] \tag{9}$$

is solved for λ_i and $\dot{v}_i$. The buckling modes are normalized using the orthogonality condition

$$\Phi_b''' \hat{u}\dot{v}_i\dot{v}_j = 0 \quad , \quad \forall i, j = 1 \ldots m \tag{10}$$

where Φ_b''' is the third Fréchet derivative evaluated at λ_b, with λ_b an appropriate reference value for the cluster (e.g. the smallest λ_i or their mean value).

- Third, the *quadratic corrections* that define the space $\mathcal{W} = \{w : w \perp \dot{v}_i, \ i = 1 \ldots m\}$, i.e. orthogonal to the space of buckling modes, are evaluated by the condition

$$w \perp \dot{v}_i \quad \Leftrightarrow \quad \Phi_b''' \hat{u}\dot{v}_i w = 0. \tag{11}$$

By defining $\xi_0 = (\lambda - \lambda_b)$ and $\dot{v}_0 = \hat{u}$, the asymptotic approximation for any equilibrium path is approximated by an expansion in terms of mode amplitudes ξ_j,

$$u[\lambda, \xi_k] = u_b + \sum_{i=0}^{m} \xi_i \dot{v}_i + \frac{1}{2} \sum_{i,j=0}^{m} \xi_i \xi_j w_{ij} \tag{12}$$

where $w_{ij} \in \mathcal{W}$ are quadratic corrections introduced to satisfy the projection of the equilibrium equation onto $\mathcal{W}$, obtained by the linear *orthogonal equations*

$$\delta w^T (K_b w_{ij} + p_{ij}) = 0 , \quad \forall w \in \mathcal{W} \tag{13}$$

where K_b is the stiffness matrix evaluated at λ_b and vectors p_{ij} are defined as a function of modes $\dot{v}_i$, $i = 0 \ldots m$, and by energy equivalence $\delta w^T p_{ij} = \Phi_b''' \delta w \dot{v}_j \dot{v}_j$.

- Fourth, the energy terms:

$$C_{ik} = \Phi_b'' w_{00} w_{ik}, \quad \mathcal{A}_{ijk} = \Phi_b''' \dot{v}_i \dot{v}_j \dot{v}_k, \quad \mathcal{B}_{ijhk} = \Phi_b'''' \dot{v}_i \dot{v}_j \dot{v}_h \dot{v}_k - \Phi_b''(w_{ij} w_{hk} + w_{ih} w_{jk} + w_{ik} w_{jh}) \tag{14}$$

are evaluated for $i, j = 0 \ldots m, k = 1 \ldots m$.

- Finally, the equilibrium path is recovered by solving the nonlinear algebraic system

$$\frac{1}{2}\sum_{i,j=0}^{m}\xi_i\xi_j\mathcal{A}_{ijk} + \frac{1}{6}\sum_{i,j,h=0}^{m}\xi_i\xi_j\xi_h\mathcal{B}_{ijhk} + \mu_k[\lambda] - \lambda_b(\lambda - \frac{1}{2}\lambda_b)\sum_{i=0}^{m}\xi_i C_{ik} = 0 \ , \quad k = 1\dots m \qquad (15)$$

of m equations in $m + 1$ unknowns $\xi_0, \xi_1 \dots \xi_m$, where

$$\mu_k[\lambda] = \frac{1}{2}\lambda_b(\lambda - \frac{1}{2}\lambda_b)\Phi_b'''\hat{u}^2\dot{v}_k + \frac{1}{6}\lambda_b^2(\lambda_b - 3\lambda)\Phi_b''''\hat{u}^3\dot{v}_k \qquad (16)$$

are *implicit imperfection factors* by the 4th order expansion of the unbalanced work on the fundamental path (i.e. $\mu_k[\lambda] = (\lambda p - s[\lambda\hat{u}])\,\dot{v}_k$).

Geometrical $\tilde{u}$ and/or load $\tilde{p}$ imperfections can be imposed on the equilibrium path by simply changing the definition of the imperfection factors $\mu_k[\lambda]$ and subsequently solving Eq. (15). As a result, computationally efficient imperfection sensitivity analyses can be performed by coupling the asymptotic method with a Monte Carlo generator (see [10, 23]). In this manner, thousands of imperfections can be tested, and those that influence the load carrying capacity of the structure the most are readily identified (see, for example, [10, 23]).

3. MIXED FORMULATION FOR VAT: LINEAR SHELL ELEMENT

The strain energy Eq. (1) of the 3D linear shell model is written in mixed form as a function of stress resultants and displacements defined on a reference surface of the plate (e.g. the mid plane). Under the assumptions of first-order shear deformation theory (FSDT), i.e. plane sections remaining plane but not necessarily perpendicular to the reference surface, and by defining a Cartesian reference system $\{X, Y, Z\}$ with the Z-axis pointing in the thickness direction, the mixed strain energy of the plate is written as:

$$\Phi[t, d] = \int_\Omega \left\{ t^T D d - \frac{1}{2} t^T E^{-1} t \right\} d\Omega \qquad t = \begin{bmatrix} t_m \\ t_f \end{bmatrix}, \quad d = \begin{bmatrix} d_m \\ d_f \end{bmatrix}, \quad D = \begin{bmatrix} D_m & 0 \\ 0 & D_f \end{bmatrix} \qquad (17)$$

where Ω is the two-dimensional domain of the reference surface, vectors t_m and t_f are the membrane stress resultants and the bending/shear stress resultants, respectively,

$$t_m = \begin{bmatrix} N_x \\ N_y \\ N_{xy} \end{bmatrix}, \quad t_f = \begin{bmatrix} t_b \\ t_s \end{bmatrix} \quad \text{with} \quad t_b = \begin{bmatrix} M_x \\ M_y \\ M_{xy} \end{bmatrix} \quad \text{and} \quad t_s = \begin{bmatrix} S_x \\ S_y \end{bmatrix} \qquad (18)$$

where t_b are bending moments and t_s shear forces. The vectors d_m and d_f are the in- and out-of-plane generalized displacements in the Cartesian reference system,

$$d_m = \begin{bmatrix} d_x \\ d_y \end{bmatrix}, \quad d_f = \begin{bmatrix} d_z \\ \varphi_x \\ \varphi_y \end{bmatrix} \qquad (19)$$

and the differential operators $\boldsymbol{D}_m$ and $\boldsymbol{D}_f$ are defined as

$$\boldsymbol{D}_m = \begin{bmatrix} \partial/\partial X & 0 \\ 0 & \partial/\partial Y \\ \partial/\partial Y & \partial/\partial X \end{bmatrix}, \quad \boldsymbol{D}_f = \begin{bmatrix} 0 & 0 & -\partial/\partial X \\ 0 & \partial/\partial Y & 0 \\ 0 & \partial/\partial X & -\partial/\partial Y \\ \partial/\partial X & 0 & 1 \\ \partial/\partial Y & -1 & 0 \end{bmatrix}. \tag{20}$$

The laminate constitutive matrix $\boldsymbol{E}$ relating reference surface stress resultants to strains is written as

$$\boldsymbol{E} = \begin{bmatrix} \boldsymbol{E}_m & \boldsymbol{E}_{mb} & \boldsymbol{0} \\ & \boldsymbol{E}_b & \boldsymbol{0} \\ \text{sym.} & & \boldsymbol{E}_s \end{bmatrix}, \quad \begin{cases} \boldsymbol{E}_m = \sum_{k=1}^{n}(Z_k - Z_{k-1})\boldsymbol{E}_m^{(k)}, & \boldsymbol{E}_{mb} = \frac{1}{2}\sum_{k=1}^{n}(Z_k^2 - Z_{k-1}^2)\boldsymbol{E}_m^{(k)} \\ \boldsymbol{E}_b = \frac{1}{3}\sum_{k=1}^{n}(Z_k^3 - Z_{k-1}^3)\boldsymbol{E}_m^{(k)}, & \boldsymbol{E}_s = \boldsymbol{\kappa} \odot \sum_{k=1}^{n}(Z_k - Z_{k-1})\boldsymbol{E}_s^{(k)} \end{cases} \tag{21}$$

where layer k is one of n total number of layers; Z_k, Z_{k-1} are the top and bottom coordinates of the k-th lamina, respectively; $\boldsymbol{E}_m^{(k)}, \boldsymbol{E}_s^{(k)}$ are the reduced lamina constitutive matrices referring to in-plane and transverse shear stress/strain, respectively, and account for the plane-stress condition in Z, and, for VAT lamina, are functions of coordinates (X, Y) (e.g. $\boldsymbol{E}_m^{(k)} = \boldsymbol{E}_m^{(k)}(X, Y)$, $\boldsymbol{E}_s^{(k)} = \boldsymbol{E}_s^{(k)}(X, Y)$, etc.). Finally, symbol $\odot$ denotes the component product that allows different shear correction factors to be introduced for each component of the $\boldsymbol{E}_s$ matrix

$$\boldsymbol{\kappa} = \begin{bmatrix} \kappa_{11} & \kappa_{12} \\ \kappa_{12} & \kappa_{22} \end{bmatrix} \tag{22}$$

3.1. SHELL FINITE ELEMENT

The mixed strain energy Eq. (17) is interpolated using the MISS-4 3D shell finite element formulation introduced by [48]. The geometry of the element is described by four nodal coordinates on the plane $Z = 0$ of the global Cartesian system $\{X, Y, Z\}$ (see Fig. 1).
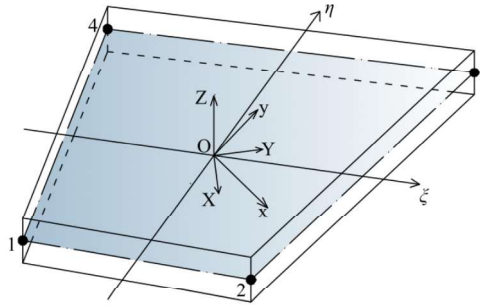

Figure 1: Global, local and internal coordinate systems.

In standard finite element notation a dimensionless internal system is defined over the element mid surface with $\{\xi, \eta\}$, $-1 \leq \xi \leq 1, -1 \leq \eta \leq 1$, which is implicitly defined by

$$\begin{cases} X = a_0 + a_1\xi + a_2\xi\eta + a_3\eta \\ Y = b_0 + b_1\xi + b_2\xi\eta + b_3\eta \end{cases} \quad \text{with} \quad \begin{bmatrix} a_0 & b_0 \\ a_1 & b_1 \\ a_2 & b_2 \\ a_3 & b_3 \end{bmatrix} = \frac{1}{4}\begin{bmatrix} 1 & 1 & 1 & 1 \\ -1 & 1 & 1 & -1 \\ 1 & -1 & 1 & -1 \\ -1 & -1 & 1 & 1 \end{bmatrix}\begin{bmatrix} X_1 & Y_1 \\ X_2 & Y_2 \\ X_3 & Y_3 \\ X_4 & Y_4 \end{bmatrix} \tag{23}$$

and $\{X_i, Y_i\}$, $i = 1, \ldots, 4$ are the global nodal coordinates.

A third local Cartesian system $\{x, y\}$ is defined over the element mid surface, centered and aligned with the element. To define this local system, we introduce the Jacobian matrix $\mathbf{J}^G$ and its average $\bar{\mathbf{J}}^G$,

$$
\mathbf{J}^G = \begin{bmatrix} X_{,\xi} & X_{,\eta} \\ Y_{,\xi} & Y_{,\eta} \end{bmatrix} = \begin{bmatrix} (a_1 + a_2\eta) & (a_3 + a_2\xi) \\ (b_1 + b_2\eta) & (b_3 + b_2\xi) \end{bmatrix}, \quad \bar{\mathbf{J}}^G = \frac{1}{4} \int_{\xi=-1}^{1} \int_{\eta=-1}^{1} \mathbf{J}^G \, \mathrm{d}\xi \, \mathrm{d}\eta = \begin{bmatrix} a_1 & a_3 \\ b_1 & b_3 \end{bmatrix}. \tag{24}
$$

The average Jacobian $\bar{\mathbf{J}}^G$ is decomposed into an orthogonal matrix $\mathbf{R}$ and a symmetric matrix $\bar{\mathbf{J}}$, so that

$$
\bar{\mathbf{J}}^G = \mathbf{R}\,\bar{\mathbf{J}}, \quad \mathbf{R} = \begin{bmatrix} \cos\alpha & -\sin\alpha \\ \sin\alpha & \cos\alpha \end{bmatrix}, \quad \alpha = \arctan\left(\frac{a_3 - b_1}{a_1 + b_3}\right), \quad \bar{\mathbf{J}} = \begin{bmatrix} a & c \\ c & b \end{bmatrix}. \tag{25}
$$

The local Cartesian system $\{x, y\}$ has its origin at the element centroid ($\xi = \eta = 0$) and is rigidly rotated by $\mathbf{R}$ with respect to $\{X, Y\}$. Thus, the coordinates $\{x, y\}$ are defined according to the transformation

$$
\begin{bmatrix} x \\ y \end{bmatrix} = \mathbf{R}^T \begin{bmatrix} X - a_0 \\ Y - b_0 \end{bmatrix} \tag{26}
$$

3.1.1. Assumed stresses

The stresses are assumed to be self-equilibrated and isostatic, leading to a minimum set of parameters, which are the 18 components of the vector $\boldsymbol{\beta}_e$. In this manner, the stress resultants are written as

$$
\mathbf{t} = \mathbf{B}\boldsymbol{\beta}_e = \begin{bmatrix} \mathbf{B}_m & \mathbf{0} \\ \mathbf{0} & \mathbf{B}_f \end{bmatrix} \begin{bmatrix} \boldsymbol{\beta}_m \\ \boldsymbol{\beta}_f \end{bmatrix} \tag{27a}
$$

where $\mathbf{B}_m$ and $\mathbf{B}_f$ are matrices representing the assumed stress modes for the membrane and flexural generalized stresses, respectively, and $\boldsymbol{\beta}_m, \boldsymbol{\beta}_f$ are 9-component vectors representing membrane and flexural moments, respectively. For the membrane stresses, it is assumed that

$$
\mathbf{B}_m = \begin{bmatrix} 1 & 0 & 0 & y & 0 & x & 0 & y^2 & -2\,a^2\,x\,y \\ 0 & 1 & 0 & 0 & x & 0 & y & -x^2 & 2\,b^2\,x\,y \\ 0 & 0 & 1 & 0 & 0 & -y & -x & 0 & a^2\,y^2 - b^2\,x^2 \end{bmatrix} \tag{27b}
$$

For the flexural stress, it is assumed that

$$
\mathbf{B}_f = \begin{bmatrix} \mathbf{B}_b \\ \mathbf{B}_s \end{bmatrix} \quad \text{with} \quad \begin{cases} \mathbf{B}_b = \begin{bmatrix} 1 & 0 & 0 & x & 0 & y & 0 & xy & 0 \\ 0 & 1 & 0 & 0 & x & 0 & y & 0 & xy \\ 0 & 0 & 1 & 0 & y\bar{c} & x/\bar{c} & 0 & 0 & 0 \end{bmatrix} \\[2ex] \mathbf{B}_s = \begin{bmatrix} 0 & 0 & 0 & -1 & -\bar{c} & 0 & 0 & -y & 0 \\ 0 & 0 & 0 & 0 & 0 & -1/\bar{c} & -1 & 0 & -x \end{bmatrix} \end{cases} \tag{27c}
$$

with $\bar{c} = a^2/b^2$.

3.1.2. Assumed displacements

The interpolation of the displacement field $\mathbf{d}$ is controlled by the 24-component vector $\mathbf{d}_e$, collecting displacements and rotations of the four nodes of the element. As the stress assumption is inherently equilibrated, the internal work can be obtained by integrating on the element contour. Therefore, only contour displacements are needed. The displacement interpolation $\mathbf{d}_k$ along element side k is defined as the sum of three contributions

$$
\mathbf{d}_k[\zeta] = \mathbf{d}_{kl}[\zeta] + \mathbf{d}_{kq}[\zeta] + \mathbf{d}_{kc}[\zeta] \tag{28a}
$$

where $-1 \leq \zeta \leq 1$ is a one-dimensional coordinate along element side k. The first term is a linear expansion

$$d_{kl}[\zeta] = \frac{1}{2}[(1-\zeta)\boldsymbol{d}^i + (1+\zeta)\boldsymbol{d}^j], \quad \begin{cases} \boldsymbol{d}^i = [d^i_x, d^i_y, d^i_z]^T \\ \boldsymbol{d}^j = [d^j_x, d^j_y, d^j_z]^T \end{cases} \tag{28b}$$

where superscripts i, j denote the nodes of element side k. The second and third terms correspond to quadratic and cubic expansions of the normal component of the element side displacements

$$d_{kq}[\zeta] = \frac{1}{8} L_k(\zeta^2 - 1) \begin{bmatrix} (\varphi^i_z - \varphi^j_z)\,\boldsymbol{n}_k \\ -(\boldsymbol{\varphi}^i - \boldsymbol{\varphi}^j)^T \boldsymbol{n}_k \end{bmatrix}, \quad d_{kc}[\zeta] = \frac{1}{4} L_k(\zeta - \zeta^3) \begin{bmatrix} \boldsymbol{n}_k \\ 0 \end{bmatrix} \theta \tag{28c}$$

with nodal rotations around the X- and Y-axes collected in

$$\boldsymbol{\varphi}^i = [\varphi^i_x, \varphi^i_y]^T \quad , \quad \boldsymbol{\varphi}^j = [\varphi^j_x, \varphi^j_y]^T \tag{28d}$$

and where $\boldsymbol{n}_k = [n_{kx}, n_{ky}]^T$ is the normal to the element side, L_k is the side length, and θ is the average in-plane distortional rotation defined as

$$\theta = \frac{1}{4} \sum_{i=1}^{4} \varphi^i_z - \bar{\varphi}_z \tag{28e}$$

with $\bar{\varphi}_z$ the average in-plane rigid rotation of the element

$$\bar{\varphi}_z = \boldsymbol{N}_\theta \boldsymbol{d}_{me} \tag{28f}$$

$$\boldsymbol{N}_\theta = \frac{1}{4\Omega_e} \left[-y_4 + y_3, \ x_4 - x_3, \ -y_4 + y_1, \ x_4 - x_1, \ -y_2 + y_1, \ x_2 - x_1, \ -y_3 + y_2, \ x_3 - x_2 \right]$$

where $\boldsymbol{d}_{me}$ collects the nodal displacements and rotations describing the membrane behavior, $\{x_i, y_i\}, i = 1 \ldots 4$ are the nodal coordinates in the local reference frame and Ω_e is the area of the element. By definition, the linear part $\boldsymbol{d}_{kl}$ and the quadratic part $\boldsymbol{d}_{kq}$ are continuous at the inter-element boundaries. The cubic contribution $\boldsymbol{d}_{kc}$ corresponds to an incompatible mode, which is added to avoid rank defectiveness [53]. Finally, a simple bilinear interpolation for bending rotations is used along the side

$$\boldsymbol{\varphi}_k[\zeta] = \frac{1}{2}[(1-\zeta)\boldsymbol{\varphi}_i + (1+\zeta)\boldsymbol{\varphi}_j], \quad \boldsymbol{\varphi}_k[\zeta] = [\varphi_x, \varphi_y]^T \tag{28g}$$

3.1.3. Compliance and compatibility

Introducing assumed stress (27) and assumed displacements (28) into the mixed strain energy (17), the elemental mixed strain energy Φ_e is defined as follows

$$\Phi_e = \boldsymbol{\beta}_e^T \boldsymbol{D}_e \boldsymbol{d}_e - \frac{1}{2} \boldsymbol{\beta}_e^T \boldsymbol{H}_e \boldsymbol{\beta}_e \tag{29a}$$

where $\boldsymbol{H}_e$ and $\boldsymbol{D}_e$ are the element compliance matrix and the compatibility matrix respectively. The compliance matrix can be written as follows

$$\boldsymbol{H}_e = \begin{bmatrix} \boldsymbol{H}_m & \boldsymbol{H}_{mb} & \boldsymbol{0} \\ & \boldsymbol{H}_b & \boldsymbol{0} \\ \text{sym} & & \boldsymbol{H}_s \end{bmatrix} \tag{29b}$$

where

$$\boldsymbol{H}_m = \int_{\Omega_e} \left\{ \boldsymbol{B}_m^T \boldsymbol{E}_m^{-1} \boldsymbol{B}_m \right\} \mathrm{d}\Omega, \quad \boldsymbol{H}_{mb} = \int_{\Omega_e} \left\{ \boldsymbol{B}_m^T \boldsymbol{E}_{mb}^{-1} \boldsymbol{B}_b \right\} \mathrm{d}\Omega \tag{29c}$$

and

$$H_b = \int_{\Omega_e} \left\{ B_b^T E_b^{-1} B_b \right\} \mathrm{d}\Omega, \quad H_s = \int_{\Omega_e} \left\{ B_s^T E_s^{-1} B_s \right\} \mathrm{d}\Omega \tag{29d}$$

The integration is performed assuming E_m, E_{mb}, E_b and E_s are constant over each individual element domain Ω_e but can change between different domains to represent VAT fiber variations. Since the compatibility matrix is due to self-equilibrated stress interpolation, and it is evaluated through analytical contour integration. It can be written as follows

$$D_e = \begin{bmatrix} D_m & 0 \\ 0 & D_f \end{bmatrix}, \quad D_m = \sum_{k=1}^{4} D_{mk} + D_c, \quad D_f = \sum_{k=1}^{4} D_{fk} \tag{29e}$$

where the matrices D_{mk} and D_{fk} are defined as

$$\beta_m^T D_{mk} d_{me} = \int_{-1}^{1} t_m^T[\zeta] N_{mk}^T d_{mk}[\zeta] \, \mathrm{d}\zeta$$

$$\beta_m^T D_c d_{me} = \int_{-1}^{1} t_m^T[\zeta] N_{mk}^T d_c[\zeta] \, \mathrm{d}\zeta$$

$$\beta_f^T D_{fk} d_{fe} = \int_{-1}^{1} t_f^T[\zeta] N_{fk}^T d_{fk}[\zeta] \, \mathrm{d}\zeta \tag{29f}$$

and the vectors d_{me} and d_{fe} collect the nodal displacements and rotations describing the membrane and flexural behaviour, respectively. Finally, the matrices N_{mk}, N_{fk} split the components of the normal to the element side,

$$N_{mk} = \begin{bmatrix} n_{kx} & 0 & n_{ky} \\ 0 & n_{ky} & n_{kx} \end{bmatrix}, \quad N_{fk} = \begin{bmatrix} 0 & 0 & 0 & n_{kx} & n_{ky} \\ n_{kx} & n_{ky} & 0 & 0 & 0 \\ -n_{ky} & 0 & -n_{kx} & 0 & 0 \end{bmatrix}. \tag{29g}$$

4. GEOMETRICAL NONLINEAR FORMULATION BASED ON COROTATIONAL APPROACH

A linear finite element can be made geometrically nonlinear using corotational algebra to describe the rigid body motion [20]. With respect to the fixed frame $\{e_1, e_2, e_3\}$, a corotational (CR) frame $\{\bar{e}_1, \bar{e}_2, \bar{e}_3\}$ is defined as

$$\bar{e}_k = Q[\alpha] e_k, \quad k = 1 \ldots 3 \tag{30}$$

with Q being a rigid rotation, parametrized by the rotation vector α according to Rodrigues' formulation [54]. The origin of the CR frame is translated by vector c. Denoting the displacement and rotation associated with position X in the fixed reference frame by d and R, respectively, the displacement and rotation in the CR frame $\bar{d}$ and $\bar{R}$ are

$$\bar{d} = Q^T(X + d - c) - X \quad, \quad \bar{R} = Q^T R. \tag{31}$$

Using a vector parametrization for $\bar{R}$ and R, and denoting the rotation vectors by $\bar{\psi}$ and ψ, we have

$$\bar{\psi} = \log(\bar{R}[\bar{\psi}]) = \log(Q^T[\alpha] R[\psi]). \tag{32}$$

A CR frame can be defined for each element by means of the element rotation vector α_e, which is a function of the element kinematical parameters d_e in the fixed frame, i.e.

$$\alpha_e = \alpha_e[d_e]. \tag{33}$$

The local kinematical parameters $\bar{d}_e$ in the CR frame are related to d_e by the geometrical transformation

$$\bar{d}_e = g[d_e] \tag{34}$$

where g collects the CR transformations for displacements Eq. (31) and rotations Eq. (32) conveniently rearranged once the definition of local kinematic parameters $\bar{d}_e$ of the finite element is fixed.

Based on the above relations, the linear finite element characterized by energy Eq. (29a) can be transformed into a geometrically nonlinear element simply by introducing a corotational description and assuming that the element kinematical parameters in Eq. (29a) are referred to the corotational frame. This leads to:

$$\Phi_e[t_e, d_e] = t_e^T D_e g[d_e] - \frac{1}{2} t_e^T H_e t_e. \tag{35}$$

The strain energy in each element can be expressed in terms of the unknown vector

$$u_e = \{t_e, d_e\}^T \tag{36}$$

which collects all parameters that define the configuration of the element in a single vector, and can be related to the global configuration vector u through the standard finite element assemblage procedure

$$u_e = A_e u \tag{37}$$

where the matrix A_e implicitly contains the connectivity constraints between elements. For the Hellinger-Reissner formulation used here, the components of u are the nodal global displacements/rotations and stress resultants.

4.1. Taylor's expansion of corotational kinematics

The corotational approach is very convenient for expressing the strain energy variations because the nonlinearity is restricted to the geometrical relationship $g[d_e]$, i.e. Eq. (34). The Taylor expansion of this relationship can be written as

$$g[d_e] = g_1[d_e] + \frac{1}{2} g_2[d_e, d_e] + \frac{1}{6} g_3[d_e, d_e, d_e] + \frac{1}{24} g_4[d_e, d_e, d_e, d_e] + \cdots \tag{38}$$

where g_n are n–multilinear symmetric forms which express the n-th Fréchet derivatives of the function $g[d_e]$. In the following, vector u_i ($i = 1 \ldots 4$) denotes a generic variation of the global finite element configuration vector of stress and displacement parameters, and vector $u_{ei} = A_e u_i = \{t_{ei}, d_{ei}\}^T$ the corresponding vector at the element level. Using the same notation u_0 and u_{e0} are the global and element reference configuration vectors.

4.2. Second-order energy variations

Second–order energy variations are used in the evaluation of the fundamental equilibrium path and the buckling modes. In both cases, using expansion Eq. (38) and the energy expression Eq. (35), the elemental energy contribution can be expressed as

$$\Phi_e'' u_{e1} u_{e2} = t_{e1}^T D_e g_1[d_{e2}] + t_{e2}^T D_e g_1[d_{e1}] - t_{e1}^T H_e t_{e2} + t_{e0}^T D_e g_2[d_{e1}, d_{e2}]. \tag{39}$$

Introducing matrices L_1 and $G[t_e]$ through the following equivalences

$$L_1 d_{ej} = g_1[d_{ej}] \quad , \quad d_{e1}^T G[t_{e0}] d_{e2} = t_{e0}^T D_e g_2[d_{e1}, d_{e2}], \tag{40}$$

Eq. (39) can be rearranged in a more compact form:

$$u_{e1}^T \Phi_e'' u_{e2} = u_{e1}^T K_e u_{e2} \quad , \quad K_e = \begin{bmatrix} -H_e & D_e L_1 \\ L_1^T D_e^T & G[t_{e0}] \end{bmatrix}. \tag{41}$$

The mixed elemental tangent stiffness matrix K_e can be used directly through a standard assemblage process to obtain the overall stiffness matrix K

$$u_1^T \Phi'' u_2 = u_1^T K u_2 \quad , \quad K = \sum_e A_e^T K_e A_e \tag{42}$$

4.3. Third and fourth order variations

Third-order energy variations are used in Koiter's approach to evaluate the third-order coefficients and are also used to evaluate the secondary force vectors (see Eq. (13) and Eq. (14)). The element contribution to the scalar coefficients can be easily calculated using the general formula

$$\Phi_e''' u_{e1} u_{e2} u_{e3} = t_{e1}^T D_e g_2[d_{e2}, d_{e3}] + t_{e2}^T D_e g_2[d_{e3}, d_{e1}] + t_{e3}^T D_e g_2[d_{e1}, d_{e2}] \\ + t_{e0}^T D_e g_3[d_{e1}, d_{e2}, d_{e3}]. \tag{43}$$

Then the element contributions can be simply added to obtain the global values. On the other hand, taking advantage of the above expression, the element contribution to the secondary force vector is evaluated by

$$\Phi_e''' u_{e1} u_{e2} = p_e = \begin{bmatrix} D_e g_2[d_{e1}, d_{e2}] \\ G[t_{e1}]d_{e2} + G[t_{e2}]d_{e1} + q[t_{e0}, d_{e1}, d_{e2}] \end{bmatrix} \tag{44}$$

where vector q is defined according to the following condition:

$$d_{e3}^T q[t_{e0}, d_{e1}, d_{e2}] = t_{e0}^T D_e g_3[d_{e1}, d_{e2}, d_{e3}]. \tag{45}$$

Then, the overall vector is then obtained by standard finite element assembly

$$\Phi''' u_1 u_2 = \sum_e A_e^T p_e[u_{e1}, u_{e2}]. \tag{46}$$

Finally, fourth-order energy variations, used to evaluate the fourth-order coefficients (see Eq. (14)), can be computed by summing the relevant element contributions based on the following expression

$$\Phi_e'''' u_{e1} u_{e2} u_{e3} u_{e4} = t_{e1}^T D_e g_3[d_{e2}, d_{e3}, d_{e4}] + t_{e2}^T D_e g_3[d_{e3}, d_{e4}, d_{e1}] \\ + t_{e3}^T D_e g_3[d_{e4}, d_{e1}, d_{e2}] + t_{e4}^T D_e g_3[d_{e1}, d_{e2}, d_{e3}] \\ + t_{e0}^T D_e g_4[d_{e1}, d_{e2}, d_{e3}, d_{e4}]. \tag{47}$$

5. NUMERICAL RESULTS

First, the reliability and accuracy of the proposed MISS-4 finite element in predicting the post-buckling behavior of square laminated VAT plates using Koiter's asymptotic approach is tested for different boundary and loading conditions. In particular, a square plate under three loading conditions (compression, bi-axial compression and shear) is considered (see Fig. 2). The loading conditions are denoted as Test 1, Test 2, Test 3. For each loading condition, three different boundary conditions are considered: clamped (CCCC), simply supported (SSSS) and simply supported/clamped (SCSC). The plates are meshed using a grid of 100×100 elements for converged results. The length of the square plate is $l = 1.0\ m$ and the thickness of each lamina is $t = 1.272 \cdot 10^{-4}\ m$. The material properties of the plate are tabulated in Table 1 and the layer stacking

sequences (LSS) are cited in Table 2. The local fiber orientation $\theta(X)$ within a VAT lamina is presented using the standard notation of Gurdal & Olmedo [28]

$$\theta(X) = \phi + \frac{2\,(T_1 - T_0)}{L_x}|X| + T_0 \tag{48}$$

where ϕ is the rotation of the fiber paths with respect to the global X-axis, T_0 is the fiber orientation angle with respect to ϕ at the plate center ($X = 0$), and T_1 is the fiber orientation angle at the plate ends ($X = \pm L_x/2$). The LSS chosen in Table 2 are balanced and symmetric and exhibit fiber paths with variations along the longitudinal and width directions, and also at 45° to either. The chosen VAT layups do not represent optimized layups for the chosen load-cases but rather serve to demonstrate the robustness and wide applicability of the modeling approach.

To validate the present approach, comparisons have been made with a finite element solution based on the Riks path-following algorithm in the commercial finite element code ABAQUS [52]. In this case, each plate was meshed with 100×100 S4R elements, each with a unique stacking sequence to approximate the VAT layup over the planform, and an initial linear eigenvalue analysis was performed to determine possible perturbations off the fundamental path. The eigenmode corresponding to the first critical eigenvalue was then applied as an initial imperfection with a scaling factor of the order $10^{-5} - 10^{-6}$ and the full nonlinear analysis was re-run using the Riks algorithm. Comparisons are also made with a Koiter's asymptotic model implemented using the differential quadrature method (see Section 5.1). In this case a discretisation grid of 42×42 points was required for convergence.

The initial post-buckling behavior of test cases 1-3 in Fig. 2 with boundary conditions (CCCC), (SSSS) and (SCSC) are all dominated by the first buckling mode. To showcase a more complicated multi-modal case with coincident buckling loads, a long plate under uni-axial compression (Fig. 3) with stacking sequence LSS3 was tested. This example highlights the importance of a full nonlinear multi-modal analysis to capture possible interactions between different buckling modes.

Table 1: Assumed material properties.

E_1 [GPa]	E_2 [GPa]	ν_{12} [−]	G_{12} [GPa]	G_{13} [GPa]	G_{23} [GPa]
181.00	10.27	0.28	7.17	4.00	4.00

Table 2: Lamina orientations.

Plate Notation	Stacking Sequence
LSS1	$(0 \pm \langle 45|0\rangle)_{3s}$
LSS2	$(45 \pm \langle 90|0\rangle)_{3s}$
LSS3	$(90 \pm \langle 0|45\rangle)_{3s}$

5.1. Differential Quadrature Method (DQM)

Differential quadrature (DQ) is a numerical discretization technique proposed by Bellman et al. [55] that approximates the partial derivative of a functional field with respect to a specific spatial variable using a linear weighted sum of all the functional values in the domain. For example, the nth partial derivative of function $f(x)$ at the ith discretization point is

$$\frac{\partial^n f(x_i)}{\partial x^n} = A_{ij}^{(n)} f(x_j), \quad i = 1, 2, \ldots, N_p \tag{49}$$

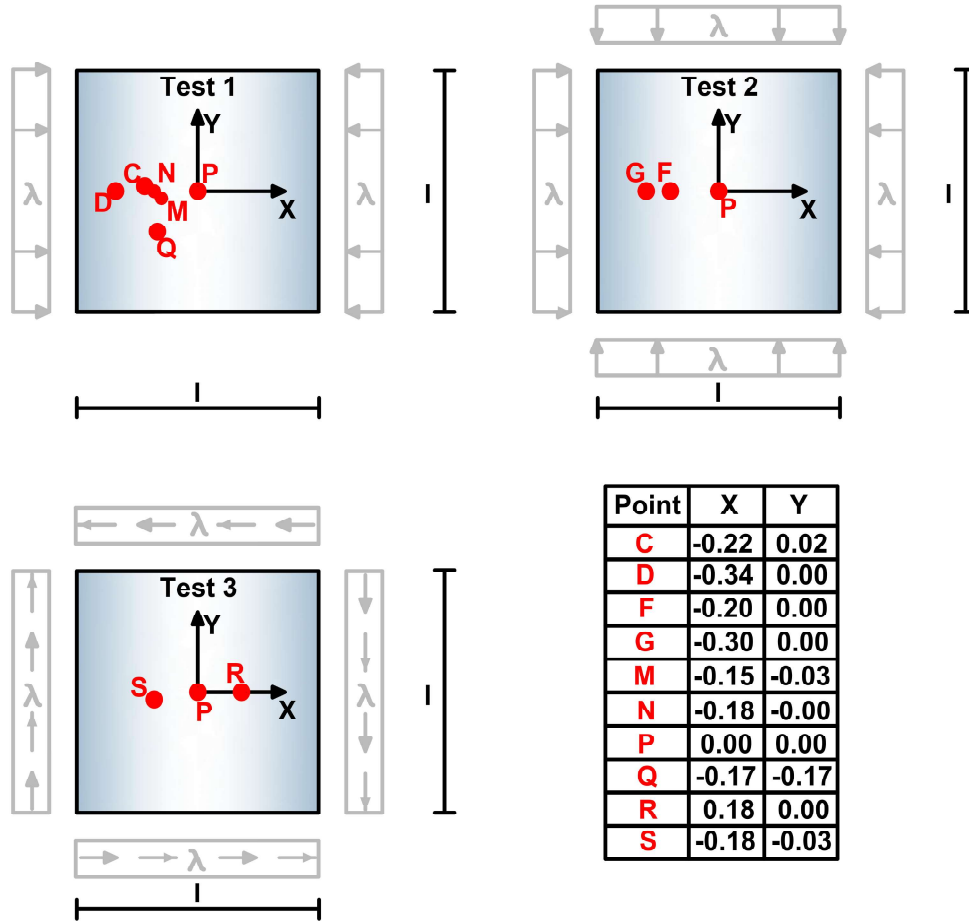| Point	X	Y
C	-0.22	0.02
D	-0.34	0.00
F	-0.20	0.00
G	-0.30	0.00
M	-0.15	-0.03
N	-0.18	-0.00
P	0.00	0.00
Q	-0.17	-0.17
R	0.18	0.00
S	-0.18	-0.03

Figure 2: Geometry of tested VAT plates and different loading conditions. In each case the edges are simply-supported. Note, even though the deformed dotted edges are depicted as straight lines, varying in-plane stiffness along an edge means that this is not necessarily so. For each test, three boundary conditions are considered (clamped (CCCC), simply supported (SSSS) and simply supported/clamped (SCSC)) and three layer stacking sequence ((LSS), see Tab. 2).

where x_i is the set of N_p discretization points in the x-direction, typically defined by the non-uniform Gauss-Lobatto-Chebychev distribution, $A_{ij}^{(n)}$ are the weighting coefficients of the nth derivative, and repeated index j means summation from 1 to N_p. The same technique is easily extended to the remaining two spatial dimensions to compute mixed derivatives.

The key to applying DQ is finding the value of the weighting coefficients for any order derivative and number of grid points. In this regard, Shu and Richard [56] proposed the generalized differential quadrature (GDQ), whereby Lagrange polynomials are used as the underlying polynomial basis for deriving $A_{ij}^{(n)}$. The interpolation coefficient matrix g_k for the Lagrangian polynomial basis [57] is given by

$$g_k(x) = \frac{m(x)}{(x - x_k)m^{(1)}(x_k)}, \quad k = 1, 2, \ldots, N_p \tag{50}$$

where

$$m(x) = \prod_{j=1}^{N_p}(x - x_j) \quad \text{and} \quad m^{(1)}(x_i) = \prod_{k=1, k \neq i}^{N_p}(x_i - x_k) \tag{51}$$
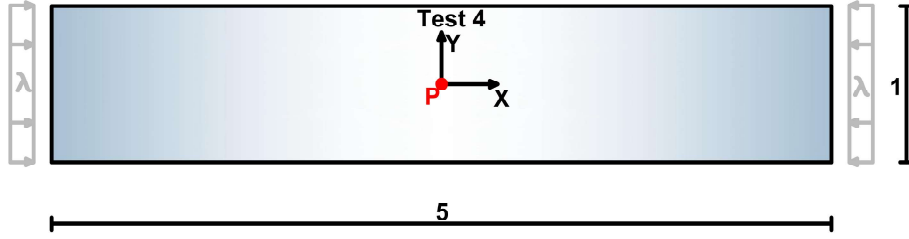
Figure 3: Geometry of a long VAT plate under uni-axial compression. All edges are simply-supported. Note, even though the deformed dotted edges are depicted as straight lines, varying in-plane stiffness along an edge means that this is not necessarily so. This test is denoted as Test 4 in the following.

and this leads to the weighting coefficients of the derivatives $A_{ij}^{(n)}$,

$$A_{ij}^{(1)} = \frac{1}{x_j - x_i} \prod_{k=1,k\neq i,j}^{N_p} \frac{x_i - x_k}{x_j - x_k} \quad \text{for} \quad i \neq j \quad \text{and} \quad A_{ii}^{(1)} = \sum_{k=1,k\neq i}^{N_p} \frac{1}{x_i - x_k}. \tag{52}$$

Subsequently, all higher-order weighting coefficients are obtained by direct matrix multiplication, i.e. $[A^{(m)}] = [A^{(1)}][A^{(m-1)}]$, with $m = 2, 3, \ldots, N_p - 1$ [58]. In this manner, any set of linear differential equations can be written as a linear system of algebraic equations by replacing the differential operators with the weighting matrix in Eq. (49). Thus, the unknown functional values $f(x_i)$ at each grid point are found by solving the strong form of the system of equations with pertinent essential or natural boundary conditions imposed on the boundary points.

5.1.1. Plate element for DQM

To model the buckling and initial post-buckling behavior of VAT panels, the classic equilibrium equations of a flat plate subjected to in-plane and transverse loading are used. The classical Kirchhoff assumptions of mid-plane normals remaining normal and unextended, and plane sections remaining plane are invoked. Thus, transverse shear strains and transverse normal strains are deemed negligible compared to their in-plane counterparts. Furthermore, Lagrangian linear kinematics with von Kármán nonlinear strains are employed [59]. Therefore,

$$\begin{cases} \dfrac{\partial N_x}{\partial X} + \dfrac{\partial N_{xy}}{\partial Y} = 0 \\[2mm] \dfrac{\partial N_y}{\partial Y} + \dfrac{\partial N_{xy}}{\partial X} = 0 \\[2mm] \dfrac{\partial^2 M_x}{\partial^2 X} + \dfrac{\partial^2 M_{xy}}{\partial X \partial Y} + \dfrac{\partial^2 M_y}{\partial^2 Y} + N_x \dfrac{\partial^2 d_z}{\partial^2 X} + 2N_{xy} \dfrac{\partial^2 d_z}{\partial X \partial Y} + N_y \dfrac{\partial^2 d_z}{\partial^2 Y} + p_z = 0 \end{cases} \tag{53}$$

where the nonlinear part of the third governing Eq. (53) represents the transverse components of the membrane forces that arise once the panel has buckled. Finally, p_z is the distributed load in the Z direction.

The membrane forces (t_m) and bending moments (t_b) per unit width in Eq. (53) are defined by

$$t_m = E_m(X, Y) \cdot (e + \eta) + E_{mb}(X, Y) \cdot \chi \qquad t_b = E_{mb}(X, Y) \cdot (e + \eta) + E_b(X, Y) \cdot \chi \tag{54}$$

where $E_m(X, Y)$, $E_{mb}(X, Y)$ and $E_b(X, Y)$ are the membrane, coupling and bending stiffness matrices of classical laminate analysis as introduced previously in Eq. (21). Note that due to the variable stiffness design of the panel, these terms are functions of location (X, Y). Finally, the linear and nonlinear membrane strains, e and η, and curvatures χ of the reference surface are given by:

$$
e = \begin{bmatrix} \partial d_x/\partial X \\ \partial d_y/\partial Y \\ \partial d_y/\partial X + \partial d_x/\partial Y \end{bmatrix}, \quad \eta = \begin{bmatrix} 1/2\,(\partial d_z/\partial X)^2 \\ 1/2\,(\partial d_z/\partial Y)^2 \\ (\partial d_z/\partial X)(\partial d_z/\partial Y) \end{bmatrix}, \quad \chi = -\begin{bmatrix} \partial^2 d_z/\partial^2 X \\ \partial^2 d_z/\partial^2 Y \\ 2\,\partial^2 d_z/\partial X \partial Y \end{bmatrix} \tag{55}
$$

where d_x, d_y, d_z are the deflections of the plate reference surface in the Cartesian $\{X, Y, Z\}$-coordinates, respectively.

Finally, the essential and natural boundary conditions that need to be applied to fully constrain the boundary value problem are

$$
\begin{cases}
d_n = \check{d}_n & \text{or} & N_{nn} = \check{N}_{nn} \\[4pt]
d_s = \check{d}_s & \text{or} & N_{ns} = \check{N}_{ns} \\[4pt]
d_z = \check{d}_z & \text{or} & Q_{nz} + \dfrac{\partial M_{ns}}{\partial s} = \check{Q}_{nz} + \dfrac{\partial \check{M}_{ns}}{\partial s} \\[8pt]
\dfrac{\partial d_z}{\partial n} = \dfrac{\partial \check{d}_z}{\partial n} & \text{or} & M_{nn} = \check{M}_{nn}
\end{cases} \tag{56}
$$

where

$$
d_n = u_x n_x + u_y n_y \qquad\qquad u_s = -u_x n_y + n_x u_y
$$
$$
\frac{\partial}{\partial n} = n_x \frac{\partial}{\partial x} + n_y \frac{\partial}{\partial y} \qquad\qquad \frac{\partial}{\partial s} = -n_y \frac{\partial}{\partial x} + n_x \frac{\partial}{\partial y}
$$
$$
N_{nn} = N_x n_x^2 + 2 N_{xy} n_x n_y + N_y n_y^2 \qquad N_{ns} = \left(N_y - N_x\right) n_x n_y + N_{xy} \left(n_x^2 - n_y^2\right)
$$
$$
Q_{nz} = \left(\frac{\partial M_x}{\partial X} + \frac{\partial M_{xy}}{\partial Y}\right) n_x + \left(\frac{\partial M_y}{\partial Y} + \frac{\partial M_{xy}}{\partial X}\right) n_y + \left(N_x \frac{\partial d_z}{\partial X} + N_{xy} \frac{\partial d_z}{\partial Y}\right) n_x + \left(N_{xy} \frac{\partial d_z}{\partial X} + N_y \frac{\partial d_z}{\partial Y}\right) n_y
$$
$$
M_{nn} = M_x n_x^2 + 2 M_{xy} n_x n_y + M_y n_y^2 \qquad M_{ns} = \left(M_y - M_x\right) n_x n_y + M_{xy} \left(n_x^2 - n_y^2\right)
$$

and the directional terms are defined by $n_x = \cos \upsilon$ and $n_y = \sin \upsilon$ where υ is the angle between the normal to the boundary and the global X-axis, and prescribed quantities on the boundary are denoted by a superimposed check symbol ˇ.

5.1.2. Koiter's solution using DQM

In Koiter's approach, the nonlinear differential Eqs. (53) are converted to an infinite set of linear differential equations. This is achieved by expanding the unknown functional fields, that for a von Kármán plate theory are $d = [d_x, d_y, d_z]^T$, in a power series of an arbitrary perturbation parameter ξ and a linear scalar λ of the external load,

$$
d[\lambda, \xi] = \lambda\,\hat{d} + \xi\,\dot{d} + \frac{1}{2}\,\xi^2\,\ddot{d} + \ldots . \tag{57}
$$

Here, the perturbation parameter is chosen to be the normalized buckling amplitude $\dot{d}_z^{max}/t$, where $\dot{d}_z^{max}$ is the amplitude of the transverse buckling mode $\dot{d}_z$, and t is the total thickness of the laminate. By combining corresponding terms of $\lambda, \xi, \xi^2, \ldots$, an infinite set of linear differential equations is obtained that represents an asymptotic series solution to the nonlinear differential equations. The first three sets of linear differential equations pertain to the pre-buckling, buckling (linear correction) and initial post-buckling (quadratic correction) solutions, respectively. These three sets of equations are solved successively for $\hat{d}, \dot{d}$ and $\ddot{d}$.

In this particular work, the applied loading conditions are purely in-plane (uni-axial compression, bi-axial compression or shear loading) and all VAT laminates are symmetrically laminated. In this case, the VAT plate remains flat in the pre-buckling regime, and the pre-buckling and initial post-buckling (quadratic

correction) responses are functions of the in-plane variables $\boldsymbol{d}_m = [d_x, d_y]^T$ only, whereas the buckling (linear correction) solution is a function of $\boldsymbol{d}_b[\xi] = d_z$ only. Thus,

$$\boldsymbol{d}_m[\lambda, \xi] = \lambda \hat{\boldsymbol{d}} + \frac{1}{2} \xi^2 \ddot{\boldsymbol{d}} \quad , \quad \boldsymbol{d}_b[\xi] = d_z = \xi \dot{d}_z. \tag{58}$$

Hence, substituting the weighting matrix of eq. (49) for the differential operators into Eq. (53), and collecting all terms associated with λ, an algebraic system of equations for the pre-buckling response is derived

$$\begin{bmatrix} A_x & 0 & A_y \\ 0 & A_y & A_x \end{bmatrix} \begin{bmatrix} \hat{N}_x \\ \hat{N}_y \\ \hat{N}_{xy} \end{bmatrix} = \begin{bmatrix} 0 \\ 0 \end{bmatrix} \quad \Rightarrow \quad A_m^T \hat{N} = 0 \tag{59}$$

where, in DQ form, the pre-buckling membrane forces are calculated as follows

$$\begin{bmatrix} \hat{N}_x \\ \hat{N}_y \\ \hat{N}_{xy} \end{bmatrix} = E_m \begin{bmatrix} A_x & 0 \\ 0 & A_y \\ A_y & A_x \end{bmatrix} \begin{bmatrix} \hat{\boldsymbol{d}}_x \\ \hat{\boldsymbol{d}}_y \end{bmatrix} \quad \Rightarrow \quad \hat{N} = E_m A_m \hat{\boldsymbol{d}} \tag{60}$$

with A_x and A_y the first-order DQ weighting matrices, and $\hat{\boldsymbol{d}}_x$ and $\hat{\boldsymbol{d}}_y$ the vectors of pre-buckling unknowns at the DQ grid points. By combining Eq. (59) and Eq. (60) we can write

$$\therefore A_m^T E_m A_m \hat{\boldsymbol{d}} = 0. \tag{61}$$

The loading condition is applied by replacing the equilibrium equations at the DQ boundary points in Eq. (59) with the appropriate essential (displacement) and natural (stress) boundary conditions of Eq. (56), which, for this particular work, include the loading conditions $N_{nn} = \check{N}_{nn}$ and $N_{ns} = \check{N}_{ns}$. As a result, some of the rows in Eq. (61) are replaced with the pertinent boundary conditions, and the null vector in Eq. (61) is replaced by a generalized load vector $\check{f}_{ext}$.

The second set of equations is a linear eigenvalue problem that yields the buckling eigenvalues λ_b and eigenmodes $\dot{d}_z$. By substituting the weighting matrix of Eq. (49) for the differential operators into Eq. (53), and collecting all terms associated with ξ, an algebraic system of equations for the generalized eigenvalue problem is derived

$$\begin{bmatrix} A_{xx} & A_{yy} & 2A_{xy} \end{bmatrix} \begin{bmatrix} \dot{M}_x \\ \dot{M}_y \\ \dot{M}_{xy} \end{bmatrix} + \lambda \begin{bmatrix} \hat{N}_x & \hat{N}_y & \hat{N}_{xy} \end{bmatrix} \begin{bmatrix} A_{xx} \\ A_{yy} \\ 2A_{xy} \end{bmatrix} \dot{d}_z = 0 \quad \Rightarrow \quad A_b^T \dot{M} + \lambda \hat{N} A_b \dot{d}_z = 0 \tag{62}$$

where $[\hat{N}_x, \hat{N}_y, \hat{N}_{xy}]^T$ are the membrane forces acting on the reference surface calculated for a prescribed unit loading in the linearized pre-buckling problem, and A_{xx}, A_{yy}, A_{xy} are the second-order DQ weighting matrices. In DQ form, the bending moments are calculated as follows

$$\begin{bmatrix} \dot{M}_x \\ \dot{M}_y \\ \dot{M}_{xy} \end{bmatrix} = E_b \begin{bmatrix} -A_{xx} \\ -A_{yy} \\ -2A_{xy} \end{bmatrix} \dot{d}_z \quad \Rightarrow \quad \dot{M} = -E_b A_b \dot{d}_z. \tag{63}$$

Thus, by combining Eq. (62) and Eq. (63), and factoring out the displacement vector $\dot{d}_z$, we are left with the generalized eigenvalue problem

$$-A_b^T E_b A_b \dot{d}_z + \lambda_b \hat{N} A_b \dot{d}_z = 0 \quad , \quad \therefore (K_0 + \lambda_b K_1) \dot{d}_z = 0 \tag{64}$$

where K_0 is the linearized stiffness matrix and K_1 the geometric stiffness matrix evaluated for the prescribed unit loading in the pre-buckling step. The the eigenvalues (buckling loads), λ_b, and eigenvectors (buckling modes), $\dot{d}_z$, are found by solving the eigenvalue problem with the appropriate essential (displacement) and natural (stress) boundary conditions replacing the rows pertaining to the boundary points.

The initial post-buckling solution $\ddot{d}$ corresponding to a particular buckling mode $\dot{d}_z$ is calculated by solving the third set of differential equations pertaining to ξ^2. Hence, substituting the weighting matrix of Eq. (49) for the differential operators into Eq. (53), and collecting all terms associated with ξ^2, an algebraic system of equations for the initial post-buckling response is derived

$$\begin{bmatrix} A_x & 0 & A_y \\ 0 & A_y & A_x \end{bmatrix} \begin{bmatrix} \ddot{N}_x \\ \ddot{N}_y \\ \ddot{N}_{xy} \end{bmatrix} = - \begin{bmatrix} A_x N_{px} + A_y N_{pxy} \\ A_x N_{pxy} + A_y N_{py} \end{bmatrix} \quad \Rightarrow \quad A_m^T \ddot{N} = \check{f}_{ext} \tag{65}$$

where the membrane forces $N_p = [N_{px}, N_{py}, N_{pxy}]^T$ are calculated from the buckling solution as follows

$$\begin{bmatrix} N_{px} \\ N_{py} \\ N_{pxy} \end{bmatrix} = E_m \begin{bmatrix} \left(A_x \dot{d}_z \right)^2 \\ \left(A_y \dot{d}_z \right)^2 \\ 2 \left(A_x \dot{d}_z \right) \left(A_y \dot{d}_z \right) \end{bmatrix} \tag{66}$$

and the initial post-buckling membrane forces $\ddot{N}$ are given by Eq. (60) with $(\hat{d}_x, \hat{d}_y)$ replaced with $(\ddot{d}_x, \ddot{d}_y)$. Thus, the initial post-buckling solution is found by solving the linear system of equations

$$A_m^T E_m A_m \ddot{d} = \check{f}_{ext} \tag{67}$$

with the appropriate essential (displacement) and natural (stress) boundary conditions imposed on the system of equations by replacing the rows pertaining to the boundary points.

After the three displacement fields $(\hat{d}, \dot{d}, \ddot{d})$ have been found, it is possible to compute the change in load factor λ for a given change in the perturbation parameter ξ. Thus, expanding the load factor in a power series in terms of ξ gives

$$\lambda = \lambda_b + \frac{1}{2} \xi^2 \ddot{\lambda} + \dots \tag{68}$$

where $\ddot{\lambda}$ is the curvature of the initial post-buckling equilibrium path. For a symmetrically laminated plate, as considered in this work, the asymmetry parameter $\dot{\lambda} = 0$ as the plate is agnostic to the direction of buckling. These path parameters can be found using the following integral expressions [60]

$$\lambda_b = \frac{1}{D} \int_\Omega \dot{M}^T \cdot \dot{\chi} \, d\Omega \quad , \quad \ddot{\lambda} = \frac{2}{D} \int_\Omega \ddot{N}^T \cdot R_p \, d\Omega \quad , \quad D = - \int_\Omega \hat{N}^T \cdot R_p \, d\Omega \tag{69a}$$

where

$$R_p = \left[\left(\frac{\partial \dot{d}_z}{\partial X} \right)^2 \quad \left(\frac{\partial \dot{d}_z}{\partial Y} \right)^2 \quad 2 \frac{\partial \dot{d}_z}{\partial X} \frac{\partial \dot{d}_z}{\partial Y} \right]^T .$$

Further details on implementing Koiter's perturbation approach in DQM are presented by White et al. [45].

5.2. Koiter's finite element analysis results

Three test cases (uni-axial compression, bi-axial compression, in-plane shear loading) with three boundary conditions (clamped (CCCC), simply supported (SSSS), simply supported/clamped (SCSC) and three different stacking sequences were analyzed comparing the MISS-4 finite element with both DQM and FE analyses. The equilibrium paths for the 27 configurations are shown in Figs. 4, 5 and 6. These graphs

show the equilibrium curves in terms of the load factor normalised by the first critical buckling load and the displacement d_z calculated at the points tabulated in Tab. 3.

For these 27 configurations the first buckling mode dominates the behavior and thus the MISS-4 and DQM asymptotic solutions are based on a single buckling mode expansion and quadratic correction (see Eq. (9) for MISS-4 and Eq. (62) for DQM). The comparison clearly shows the accuracy of the proposed analysis in recovering the equilibrium paths in the initial pre-buckling regime.

Table 3: Location of displacement d_z for the 27 configurations corresponding to the points defined in Fig. 2.

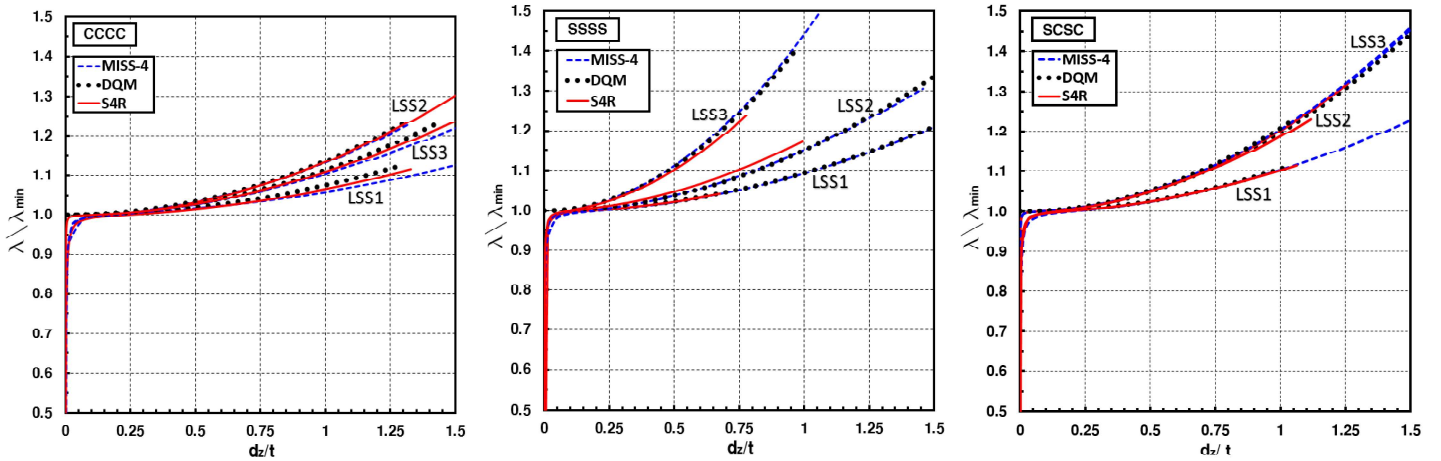|	SSSS			CCCC			SCSC		
	LSS1	LSS2	LSS3	LSS1	LSS2	LSS3	LSS1	LSS2	LSS3
Test 1	P	P	Q	P	M	N	P	C	D
Test 2	P	P	P	P	P	F	P	P	G
Test 3	P	P	P	P	P	P	P	R	S

Figure 4: Test 1: Equilibrium paths calculated using the MISS-4 element based on Koiter's asymptotic analysis, which is compared with a Koiter DQM approach and Riks path-following solutions using ABAQUS. The load factor λ is normalized by the first critical buckling load λ_{min}. Refer to Tab. 3 for the point on the plate that d_z refers to.

For the post-buckling analysis of Test 4, the first four buckling modes have been used in the expansion of quadratic correction, i.e. the initial post-buckling solution. The buckling loads ($\lambda_i, i = 1 \ldots 4$, see Eq. (9)) and modes ($\dot{v}_i, i = 1..4$) are shown in Fig. 7. The corresponding quadratic corrections ($w_{ij}, i, j = 1 \ldots 4$, see Eq. (13)) are presented in Fig. 8.

The equilibrium path, in terms of the normalized load, λ/λ_{min}, versus normalized displacement, d_z/t, is shown in Fig. 9. As the first four buckling loads are clustered together, with the first pair of modes coincident and the second pair of modes coincident, a multi-modal analysis that accounts for more than just the first buckling mode is crucially important for capturing the post-buckling path. Initially, the post-buckling behavior at point "B" in Fig. 9 is dominated by the first buckling mode. However, as we progress along the post-buckling equilibrium path, higher-order buckling modes start to contribute to the deformation (points "C", "D" and "E"). As a result, the final deformed configuration of the VAT plate at point "F" is significantly different from the first buckling mode.

The normalized modal amplification factors ξ_i/t of the first four buckling modes plotted in Fig. 10
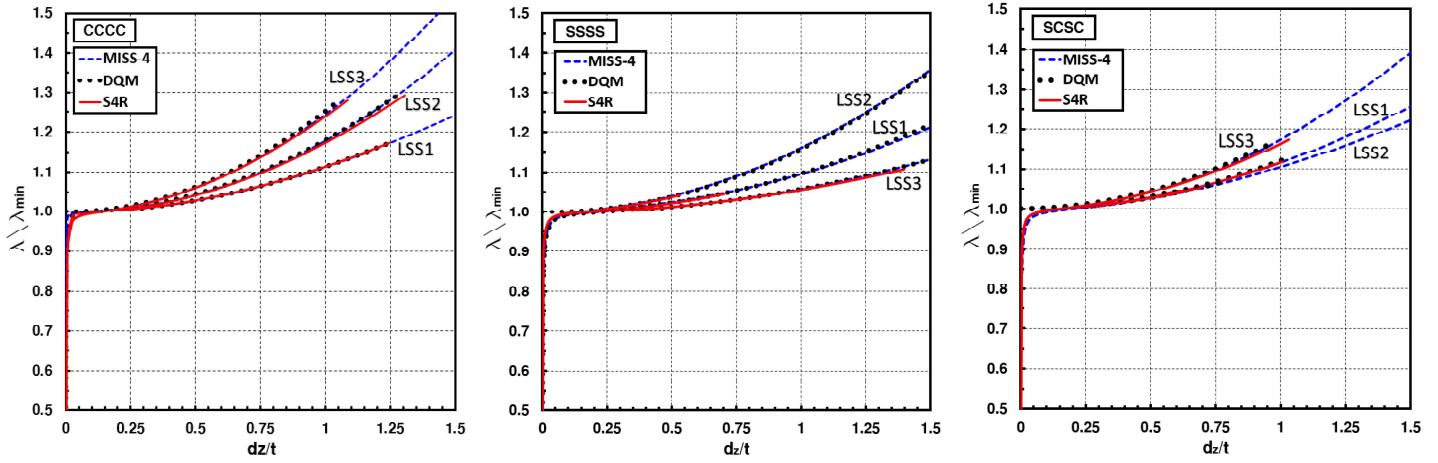
Figure 5: Test 2: Equilibrium paths calculated using the MISS-4 element based on Koiter's asymptotic analysis, which is compared with a Koiter DQM approach and Riks path-following solutions using ABAQUS. The load factor λ is normalized by the first critical buckling load λ_{min}. Refer to Tab. 3 for the point on the plate that d_z refers to.
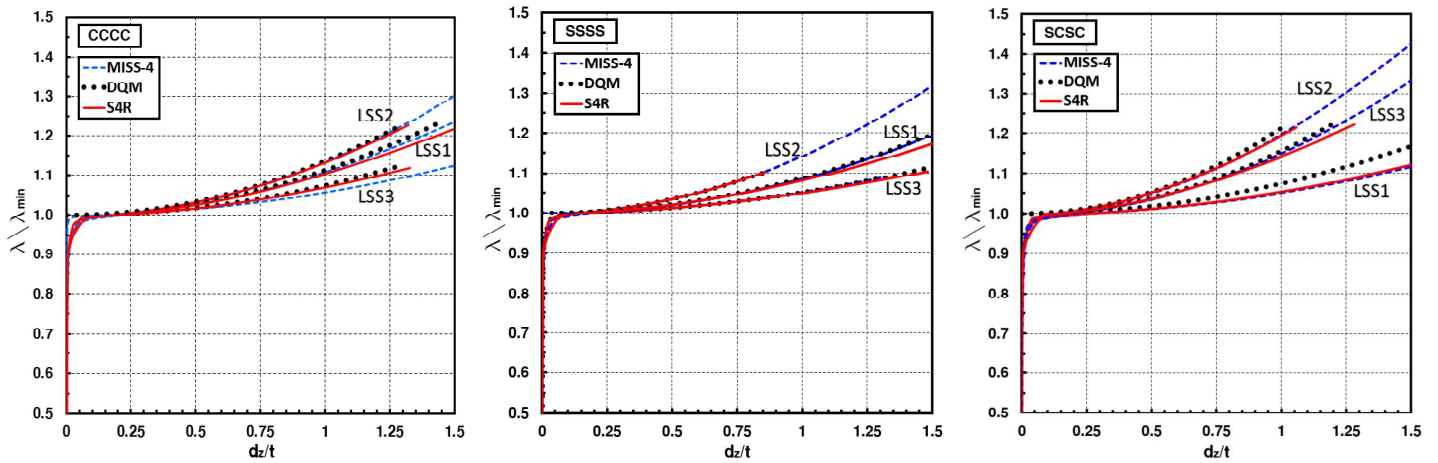

Figure 6: Test 3: Equilibrium paths calculated using the MISS-4 element based on Koiter's asymptotic analysis, which is compared with a Koiter DQM approach and Riks path-following solutions using ABAQUS. The load factor λ is normalized by the first critical buckling load λ_{min}. Refer to Tab. 3 for the point on the plate that d_z refers to.

show that the deformation along the post-buckling path is predominantly influenced by buckling modes 1 and 4, with some contribution of mode 2. While mode 1 remains the dominant contribution to the post-buckling solution, the contribution of higher-order modes can clearly not be neglected. In fact, Fig. 11 shows the convergence of the asymptotic series as the number of buckling modes in the asymptotic solution is increased from the first mode only to a multi-modal analysis incorporating the first eight modes. The plot shows that including only the first up to a combination of the first three buckling modes is not sufficient in capturing the post-buckling behavior. However, the solution sufficiently converges once the first four buckling modes are accounted for simultaneously.
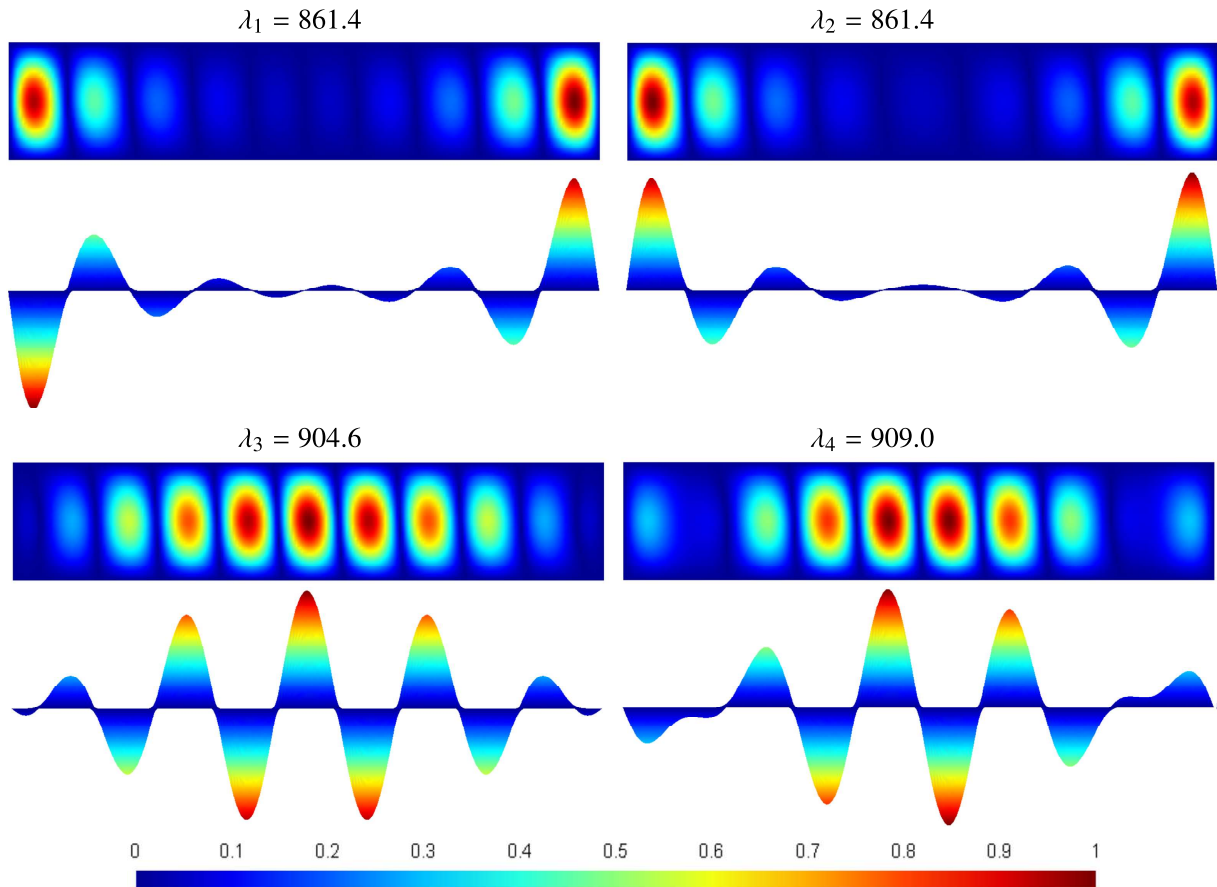

Figure 7: Test 4: The first four buckling loads λ_i and corresponding buckling modes $\dot{v}_i$, $i = 1 \dots 4$ (see Eq. (9)).

w_{11}

w_{12}

w_{13}

w_{14}

w_{22}
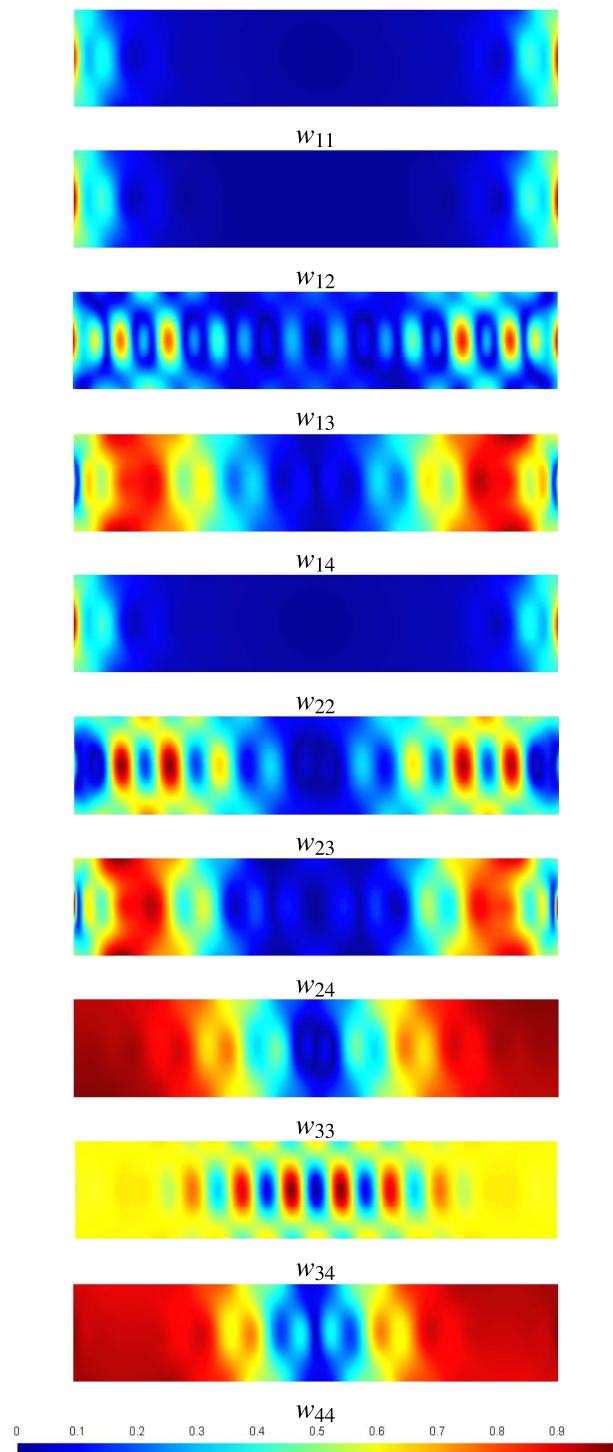
w_{23}

w_{24}

w_{33}

w_{34}

w_{44}

Figure 8: Test 4: "Heatmap" plots of the quadratic corrections ($w_{ij}, i, j = 1 \dots 4$, see Eq. (13)).
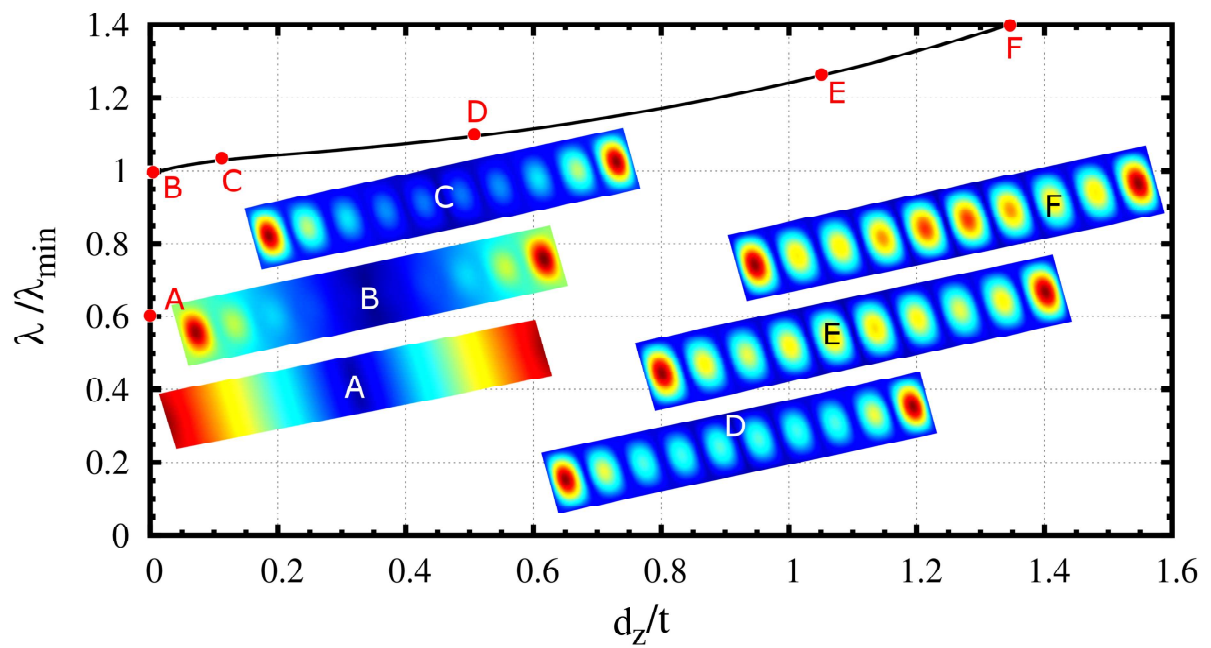
Figure 9: Test 4: Equilibrium path of normalized load λ/λ_{min} versus normalized displacement d_z/t at point "P" (see Fig. (3)). "Heat maps" of deformed equilibrium configurations at different points along the pre-critical and the post-critical path show the evolution of mode 1-dominated post-buckling behavior at point "B" to a combination of multiple modes at point "F".
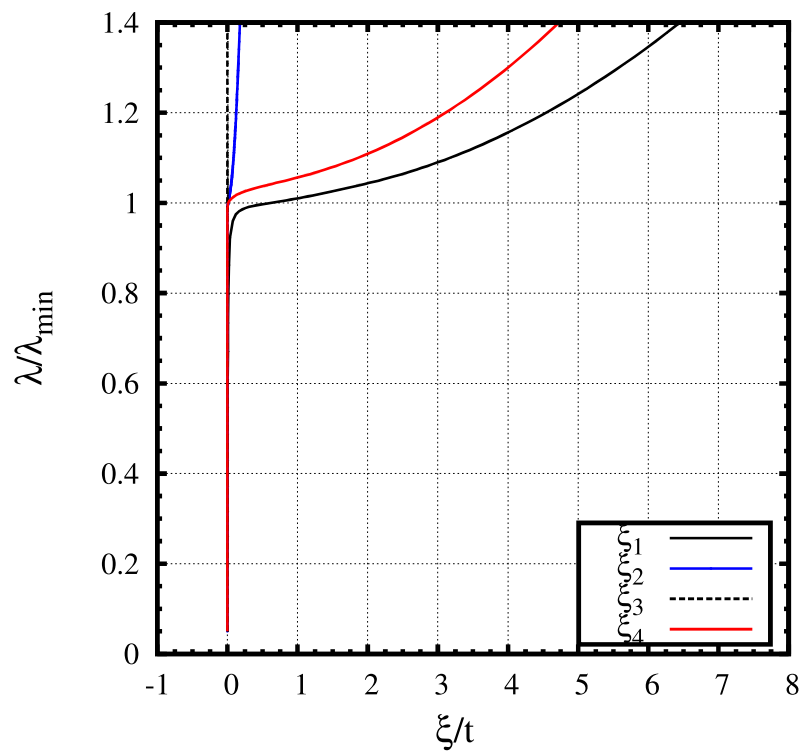
Figure 10: Test 4: Contributions of the normalized modal amplification parameters ξ_i/t of the first four buckling modes $i = 1 \ldots 4$ to the total deformed configuration along the equilibrium path. The deformation is dominated by buckling modes 1 and 4 with some contribution from mode 2.
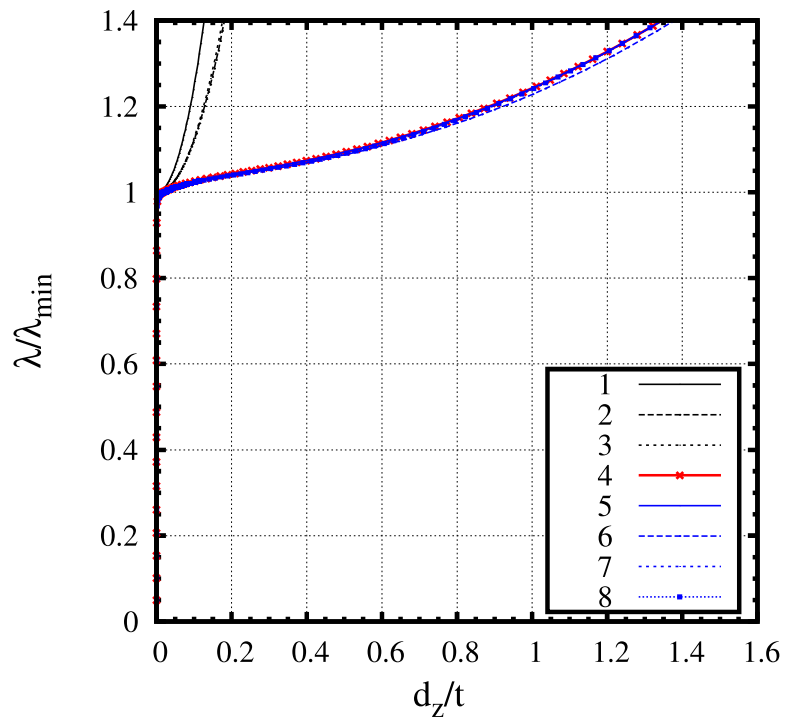
Figure 11: Test 4: Equilibrium paths of normalized load λ/λ_{min} versus normalized displacement d_z/t at point "P" (see Fig. (3)) accounting for different number of buckling modes, from a single mode 1 analysis to an eight-mode analysis. Analyses that only account up to the first three buckling modes are not sufficient in capturing the post-buckling behavior, but the analysis converges once the first four modes are accounted for in a multi-modal analysis.

6. CONCLUDING REMARKS

A robust and computationally efficient method for analyzing the post-buckling behavior of flat variable-angle tow (VAT) plates using Koiter's asymptotic approach implemented using the finite element method has been proposed. The analysis accounts for multi-modal interactions in the evaluation of the post-critical behavior. The energy variation required for the asymptotic expansion has been obtained using a corotational approach starting from the linear mixed finite element called MISS-4. The accuracy of the overall approach is documented by comparisons with an asymptotic Koiter's solution implemented within a differential quadrature framework and a path-following solution obtained using ABAQUS.

The present work has also highlighted the importance of accounting for multiple buckling modes in the quadratic correction that is used to recover the post-buckling path. For structures where the first few buckling loads are unique and not clustered, a post-buckling expansion based on the first mode may be sufficient. However, for long plates, curved shell structures or optimized structures where buckling loads are often coincident, the interaction of multiple buckling modes is crucially important when evaluating the post-critical behavior.

The proposed approach can be easily extended to other finite element formulations due to the use of a general corotational reference frame and also used as a facet element to mesh shell geometries [9, 21]. Future work will focus on analyzing the load carrying capacity VAT structures subject to initial imperfections by coupling the proposed Koiter approach with a Monte Carlo engine [10].

BIBLIOGRAPHY

[1] Koiter WT. On the stability of elastic equilibrium. 1945; English transl. NASA TT-F10, 883 (1967) and AFFDL-TR70-25 (1970).

[2] Tiso P, Abdalla MM, Jansen EL. Koiter's post-buckling analysis of general shell structures using the finite element method. In Proceedings of the 25th International Congress of the Aeronautical Sciences, Hamburg, Germany: ICAS, 1-13, 2006.

[3] Rahman T, Jansen E. Finite element based coupled mode initial post-buckling analysis of a composite cylindrical shell. Thin-Walled Struct 2010;48(1):25-32.

[4] Rahman T, Ijsselmuiden ST, Abdalla MM, Jansen EL. Postbuckling analysis of variable stiffness composite plates using a finite element-based perturbation method. Int J Str Stab Dyn 2011;11(4):735-753.

[5] Liang K, Abdalla MM, Gurdal Z. A Koiter-Newton approach for nonlinear structural analysis. Int J Numer Meth Eng 2013;96(12):763-786.

[6] Liang K, Ruess M, Abdalla MM. The Koiter-Newton approach using von Kármán kinematics for buckling analyses of imperfection sensitive structures. Comput Method Appl M 2014;279:440-468.

[7] Henrichsen SR, Weaver PM, Lindgaard E, Lund E. Post-buckling optimization of composite structures using Koiter's method. Int J Numer Meth Eng 2016, doi: 10.1002/nme.5239.

[8] Casciaro R, Mancusi G. Imperfection sensitivity due to coupled instability: a non-convex QP solution algorithm. Int J Numer Meth Eng 2006;67(6):815-840.

[9] Barbero EJ, Madeo A, Zagari G, Zinno R, Zucco G. Koiter asymptotic analysis of folded laminated composite plates. Compos Part B 2014;61:267-274.

[10] Barbero EJ, Madeo A, Zagari G, Zinno R, Zucco G. Imperfection sensitivity analysis of laminated folded plates. Thin-Walled Struct 2015;90:128-39.

[11] Cava D, Camotim D, Dinis PB, Madeo A. Numerical Investigation and Direct Strenght Design of Cold-Formed Steel Lipped Channel Columns Experiencing Local-Distortional-Global Interaction. Thin-Walled Struct 2016; 105,231-247.

[12] Zagari G, Zucco G, Madeo A, Ungureanu V, Zinno R, Dubina D. Evaluation of the erosion of critical buckling load of cold-formed steel members in compression based on Koiter asymptotic analysis. Thin-Walled Struct 2016;108:193-204.

[13] Casciaro R. Computational asymptotic post-buckling analysis of slender elastic structures. Phenomenological and Mathematical Modelling of Structural Instabilities, Springer Vienna 2005;470:195-276.

[14] Garcea G, Bilotta A, Madeo A, Casciaro R. Direct Evaluation of the Post-Buckling Behavior of Slender Structures Through a Numerical Asymptotic Formulation. Direct Methods for Limit States in Structures and Materials. 2014; 203-228.

[15] Salerno G, Lanzo D. A nonlinear beam finite element for the post-buckling analysis of plane frames by Koiter's perturbation approach. Comput Method Appl M 1997;146(3-4):325-349.

[16] Casciaro R, Salerno G, Lanzo AD. Finite element asymptotic approach of slender elastic structures: a simple approach. Int J Numer Meth Eng 1992;35(7):1397-1426.

[17] Lanzo AD, Garcea G, Casciaro R. Asymptotic post-buckling analysis of rectangular plates by HC finite elements. Int J Numer Meth Eng 1995;38(14):2325-2345.

[18] Garcea G, Madeo A, Casciaro R. The implicit corotational method and its use in the derivation of nonlinear structural models for beams and plates. J Mech Mater Struct 2012; 7(6):509–538.

[19] Garcea G, Madeo A, Casciaro R. Nonlinear FEM analysis for beams and plate assemblages based on the implicit corotational method. J Mech Mater Struct 2012;7 (6):539–574.

[20] Garcea G, Madeo A, Zagari G, Casciaro R. Asymptotic post-buckling FEM analysis using corotational formulation. Int J Solids Struct 2009;46(2):377-397.

[21] Zagari G, Madeo A, Casciaro R, de Miranda S, Ubertini F. Koiter analysis of folded structures using a corotational approach. Int J Solids Struct 2009;46(2):377-397.

[22] Barbero EJ, Madeo A, Zagari G, Zinno R, Zucco G. Imperfection sensitivity analysis of composite cylindrical shells using Koiter's method. Int J Str Stab Dyn 2016, accepted for publication.

[23] Ungureanu V, Dubina D, Crisan A, Madeo A, Zagari G, Zucco G, Zinno R. Koiter asymptotic analysis of thin-walled cold-formed steel members. Acta Mechanica et Automatica 2015 9(4):245-51.

[24] Crisan A, Ungureanu V, Dubina D. Behaviour of cold-formed steel perforated sections in compression. Part I: experimental investigations. Thin-Walled Struct 2012;61:86-96.

[25] Crisan A, Ungureanu V, Dubina D. Behaviour of cold-formed steel perforated sections in compression. Part II: numerical investigations and design considerations. Thin-Walled Struct 2012;61:97-105.

[26] Dubina D, Ungureanu V. Instability mode interaction: From van der Neut model to ECBL approach. Thin-Walled Struct 2014;81:39-49.

[27] Kubiak T, Urbaniak M, Zucco G, Madeo A. Imperfection sensitivity analysis of the nonlinear stability of composite beams-numerical and experimental investigations. Compos Part B 2016; 94:360-369.

[28] Gurdal Z, Olmedo R. In-plane response of laminates with spatially varying fiber orientations: variable stiffness concept. AIAA J, 1993;31(4):751-8.

[29] Gurdal Z, Tatting BF, Wu CK. Variable stiffness composite panels: Effects of stiffness variation on the in-plane and buckling response. Compos Part A-Appl S, 2008;39:911-922.

[30] Setoodeh S, Abdalla MM, Ijsselmuiden ST, Gurdal Z. Design of variable stiffness composite panels for maximum buckling load. Compos Struct, 2008; 87: 109-117.

[31] Lopes CS, Gurdal Z, Camanho, PP. Tailoring for strength of composite steered-fiber panels with cutouts. Compos Part A-Appl S, 2010;41:1760-1767.

[32] Wu Z, Weaver PM, Raju G, Kim BC. Buckling analysis and optimisation of variable angle tow composite plates. Thin-Walled Struct, 2012; 60: 163-172.

[33] Raju G, Wu G, Kim BC, Weaver PM. Prebuckling and buckling analysis of variable angle tow plates with general boundary conditions. Compos Struct, 2012; 94: 2961-2970.

[34] Liu W, Butler R. Buckling optimization of variable-angle-tow panels using the infinite-strip method. AIAA Journal, 2013; 51: 1442-1449.

[35] Raju G, Wu Z, Weaver PM. Buckling and postbuckling of variable angle tow composite plates under in-plane shear loading. Int J Solids Struct, 2015; 58: 270-287.

[36] Wu Z, Raju G, Weaver PM. Postbuckling analysis of varible angle tow composite plates. Int J Solids Struct, 2013; 50: 1770-1780.

[37] Wu Z, Weaver PM, Raju G. Postbuckling optimisation of variable angle tow composite plates. Compos Struct, 2013; 103: 34-42.

[38] White SC, Weaver PM. Towards imperfection insensitive buckling response of shell structures-shells with plate-like post-buckled responses. Proceedings of the 4th Aircraft Structural Design Conference of the Royal Aeronautical Society, 2014; Belfast, UK.

[39] Ijsselmuiden ST, Abdalla MM, Gurdal Z. Optimization of variable-stiffness panels for maximum buckling load using lamination parameters. J Aircraft, 2010; 48(1): 134-143.

[40] van Campen JMJF, Kassapoglou C, Gurdal Z. Generating realistic laminate fiber angle distributions for optimal variable stiffness laminates. Compos Part B, 2012; 43: 354-360.

[41] Arian Nik M, Fayazbakhsh K, Pasini D, Lessard L. Surrogate-based multi-objective optimization of a composite laminate with curvilinear fibres. Compos Struct, 2012; 94: 2306-2313.

[42] Arian Nik M, Fayazbakhsh K, Pasini D, Lessard L. Optimization of variable stiffness composites with embedded defects induced by Automated Fiber Placement. Compos Struct, 2014; 107: 160-166.

[43] Groh RMJ, Weaver PM. Buckling analysis of variable angle tow variable thickness panels with transverse shear effects. Compos Struct, 2014; 107: 482-493.

[44] Raju G, Wu Z, Weaver PM. Postbuckling analysis of variable angle tow plates using differential quadrature method. Compos Struct, 2013;106: 74-84.

[45] White SC, Raju G, Weaver PM. Initial post-buckling of variable-stiffness curved panels. J Mech Phys Solids, 2014; 71: 132-155.

[46] Groh RMJ, Weaver PM. Mass Optimization of Variable Angle Tow, Variable Thickness Panels with Static Failure and Buckling Constraints, AIAA SciTech 56th AIAA/ASCE/AHS/ASC Structures, Structural Dynamics, and Materials Conference 2015, Kissimmee, USA.

[47] Raju G, White S, Wu Z. Optimal postbuckling design of variable angle tow composites using lamination parameters. Proceedings of the 56th AIAA/ASME/ASCE/AHS/ASC Structures, Structural Dynamics and Materials Conference, 2015; Kissimmee, USA.

[48] Madeo A, Zagari G, Casciaro R, de Miranda S. A mixed 4-node 3D plate element based on self-equilibrated isostatic stresses. Int J Str Stab Dyn 2015;15(4):1450066.

[49] Barbero EJ, Madeo A, Zagari G, Zinno R, Zucco G. A mixed isostatic 24 dof element for static and buckling analysis of laminated folded plates. Compos Struct, 2014; 116: 223-234.

[50] Zucco G, Groh RMJ, Madeo A, Weaver PM. Mixed shell element for static and buckling analysis of variable angle tow composite plates. Compos Struct, 2016; 152: 324-338.

[51] Riks E. An incremental approach to the solution of snapping and buckling problems. Int J Solids Struct 1979;15(7):529-551.

[52] Dassault Systemes. Abaqus theory manual, version 6.14, 2014.

[53] Madeo A, Zagari G, Casciaro R. An isostatic quadrilateral membrane finite element with drilling rotations and no spurious modes. Finite Elem Anal Des 2012; 50:21:32.

[54] Rodrigues O. Des lois géometriques qui régissent les déplacements dun système solide dans lespace. Journal de Mathématiques Pures et Appliques 1840;5:380-440.

[55] Bellman R, Kashef G. Casti J. Differential quadrature: A technique for the rapid solution of nonlinear partial differential equations. J Comput Phys, 1972; 10: 40-52.

[56] Shu C, Richards BE. Application of generalized differential quadrature to solve two-dimensional incompressible Navier-Stokes equations. Int J Num Meth Fl, 1992; 15: 791-798.

[57] Quan JR, Chang, CT. New insights in solving distributed system equations by the quadrature method. I. Analysis. Computers & Chemical Engineering, 1989; 13(7): 779-788.

[58] Shu C. Differential Quadrature and its Application in Engineering. Springer Verlag, 2000.

[59] von Kármán, T. The Strength of Thin Plates in Compression. Transactions of the American Society of Mechanical Engineers, 1932;54: 53-57.

[60] Budiansky B. Theory of buckling and post-buckling behavior of elastic structures. Advances in Applied Mechanics, 1974; 13: 1-65.